ACADEMIA ROMÂNĂ
Revue Roumaine de Chimie
https://www.icf.ro/rrch/

Rev. Roum. Chim.,
2026, *71*(3–4), 217–223
DOI: 10.33224/rrch.2026.71.3-4.06

COMPUTATIONAL ANALYSIS OF RIBAVIRIN AND HUMAN SERUM ALBUMIN INTERACTION

Haya Mohammed Qaid ALMANSARI,[a] Saharuddin B. MOHAMAD,[b] Mujaheed ABUBAKAR,[c] Marwan Abdelmahmoud Abdelkarim MAKI,[a] Kushagra KHANNA,[a] Mogana S. RAJAGOPAL[a] and Saad TAYYAB[a*]

[a]Faculty of Pharmaceutical Sciences, UCSI University, Kuala Lumpur, Malaysia
[b]Institute of Biological Sciences, Faculty of Science, Universiti Malaya, Kuala Lumpur, Malaysia
[c]Department of Biological Sciences, Faculty of Natural and Applied Sciences, Sule Lamido University, Kafin Hausa, Nigeria

Received July 22, 2025

Ribavirin (RIB) is a broad-spectrum antiviral used to treat infections such as hepatitis C and respiratory syncytial virus. Understanding its interaction with human serum albumin (HSA), the primary plasma transport protein, is essential for optimizing pharmacokinetics and therapeutic efficacy. This study aimed to investigate the binding interaction between RIB and HSA using molecular docking and molecular dynamics (MD) simulations. Docking analysis identified Site I in subdomain IIA as the preferred binding site, with stabilization via hydrogen bonds and hydrophobic interactions. MD simulations confirmed the complex's stability over time, revealing minimal fluctuations and no significant conformational changes in HSA upon binding. These results suggest that RIB binds efficiently to HSA without compromising protein integrity, supporting its role in drug transport. The study enhances the understanding of RIB's pharmacokinetic profile and may aid in refining dosing strategies for improved clinical outcomes.

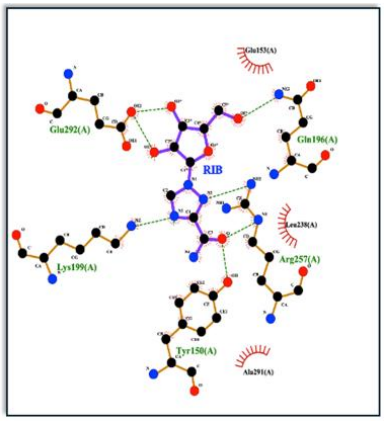

INTRODUCTION

The interaction between pharmaceuticals and plasma proteins plays a crucial role in determining the pharmacokinetics and pharmacodynamics of drugs.[1] Human serum albumin (HSA), the most abundant protein in human blood plasma, is a primary carrier for various endogenous and exogenous compounds, influencing their distribution, free concentration, and elimination.[2] Understanding the binding characteristics of drugs to HSA is essential for predicting their efficacy, dosage, and potential drug-drug interactions.[3]

Ribavirin (Fig. 1), a guanosine analogue and a broad-spectrum antiviral medication, is widely used in the treatment of various viral infections, most notably hepatitis C virus (HCV) and respiratory syncytial virus (RSV).[4,5] Chronic hepatitis C is a major global health problem, leading to severe liver diseases such as cirrhosis and hepatocellular carcinoma. Combining

* Corresponding author: saadtayyab2004@yahoo.com; Saad.Tayyab@ucsiuniversity.edu.my

ribavirin with other antiviral agents, like interferon or direct-acting antivirals, has significantly improved treatment outcomes for HCV patients.[6] Despite its therapeutic importance, the interaction of ribavirin with serum proteins, particularly HSA, remains inadequately characterized. Such interactions are critical as they affect the drug's bioavailability and therapeutic index.[7]

Computational approaches, such as molecular docking and dynamics simulations, have been widely employed to study ligand–protein interactions and assess binding site affinities, providing valuable insights into the structural determinants of ligand binding.[8] Competitive binding studies provide valuable insights into drugs' binding affinity and specificity to plasma proteins. These studies help elucidate how drugs compete with endogenous ligands and co-administered drugs for binding sites on HSA.[9] This information is pivotal for optimizing drug dosing regimens and minimizing adverse effects resulting from altered drug distribution.[10]

This study aimed to evaluate the binding interaction of RIB with HSA in order to better understand its binding affinity and potential implications for HSA's ligand-binding behavior. We utilized computational modelling to identify the binding site and understand the interaction dynamics between ribavirin and HAS. The findings from this study will contribute to a more comprehensive understanding of ribavirin's pharmacokinetics and aid in developing improved therapeutic strategies for managing HCV and other viral infections.

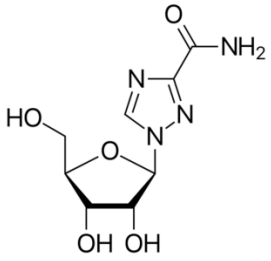

Fig. 1 – Chemical structure of Ribavirin.

EXPERIMENTAL

Molecular docking

To identify the specific drug-binding site (s) on HSA and elucidate drug-protein interactions, AutoDock 4.2 and AutoDockTools 4.2 were utilized.[11] The 3-D structure of the ligand was generated using Avogadro 1.1.1, employing the MMFF94 force field with a steepest descent algorithm for merging nonpolar hydrogens and energy minimization. The crystal structure of HSA (PDB Code: 1BM0; resolution: 2.5 Å) was obtained from the Protein Data Bank (http://www.rcsb.org/).[12,13] For the preparation of the HSA structure, water molecules were removed, polar hydrogen atoms were added, and Kollman charges were assigned to optimize computational efficiency.[14] During docking analysis, the ligand's flexibility was maintained with eight torsional degrees of freedom, and Gasteiger partial charges were assigned to all atoms. Docking simulations for Sites I, II, and III on HSA utilized specific grid boxes centred at coordinates: Site I (x = 35.3, y = 32.4, z = 36.5), Site II (x = 14.4, y = 23.6, z = 23.3), and Site III (x = 42.5, y = 24.4, z = 15.3). Each grid box had dimensions of 70 × 70 × 70 Å^3 with a spacing of 0.375 Å. The docking employed Lamarckian genetic algorithms with 250,000 energy evaluations, and cluster analysis was performed with an RMSD tolerance of 2.0 Å. Detailed visualization and analysis of binding interactions between the drug and HSA were conducted using UCSF Chimera and LigPlot+.[15,16]

Molecular dynamics (MD) simulation

The ligand-protein complex with bound RIB at Site I underwent an MD simulation. The MD simulation with GROMACS 2022 further explores ligand binding modes and elucidates the impact of ligand binding on protein conformation.[17] The simulation ran for 100 nanoseconds and employed a V-rescale thermostat and Perriello-Rahman barostat to control temperature and pressure.[18] Initially, the topology of RIB was generated using SwissParam and integrated with HSA's topology. Energy minimization was conducted using the CHARMM36 force field with the steepest descent algorithm, followed by neutralization and solvation using the TIP3P water model. The particle-net Ewald technique calculated long-range electrostatic interactions and nearest-neighbor searches.[19] Trajectory data was recorded at ten picosecond intervals throughout the simulation, yielding multiple trajectories for analysis, including the initial structure. Analysis and visualization of results were performed using the XMGrace tool, facilitating the interpretation of RIB's interactions within HSA.[20]

RESULTS AND DISCUSSION

Molecular docking results

The cluster analysis results for all binding sites, I, II, and III are depicted in Fig. 2. At Site I, seven multi-member conformations were identified, showing the lowest mean binding energy value recorded at –22.7 kJ mol^{-1} (highlighted in orange). For Sites II and III, nine and fourteen individual conformational clusters were detected, respectively, with the lowest mean binding energies noted as –19.7 kJ mol^{-1} (in green) and –21.0 kJ mol^{-1} (in pink), respectively. The most favorable binding mode, characterized by the lowest mean binding energy within the conformational clusters at Site I, was selected for subsequent analysis (Fig. 3). The binding site, defined by amino acids within a 5 Å distance from the drug, was identified deep within a hydrophobic cleft in the protein's structure, surrounded by five amino acid residues: Lys-199, Gln-196, Glu-292, Arg-257, and Tyr-150. Hydrophobic residues such as Glu153, Leu238, and Ala291 appear to stabilize the RIB–HSA complex through hydrophobic interactions. Additionally, seven hydrogen bonds were observed between the ligand, RIB, and Site I of HSA (Fig. 4, Table 1). Therefore, the preferred binding site of RIB was identified within the hydrophobic cavity of Sudlow's Site I (subdomain IIA) on HSA.

Table 1

The lowest binding energy values and predicted hydrogen bonds formed between the amino acid residue atoms of HSA(1BM0) and RIB at binding Site I as were determined by molecular docking analysis

Binding position on HSA	Residue in HSA: atom	RIB atom	Distance Å
Site I	Lys-199: H3Z	N	2.1
	Gln-196: HE2	O5	2.2
	Glu-292: H2	OE2	2.0
	Glu-292: H3	OE2	2.0
	Arg-257: 2HH2	N	2.0
	Arg-257: 2HH2	O	2.7
	Tyr-150: HH	O	1.8

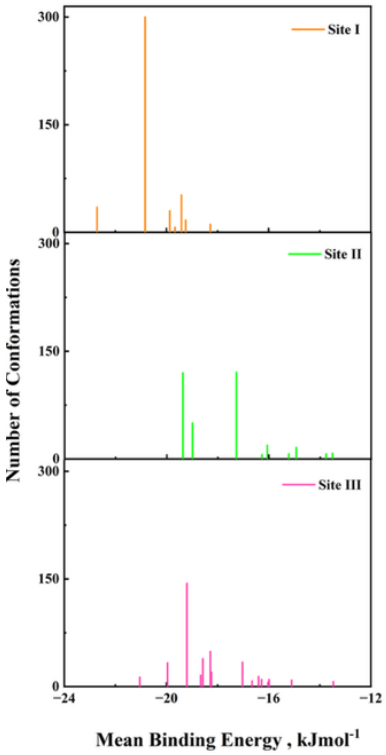

Fig. 2 – The evaluation of RIB-HSA docked complexes in the context of subdomain IIA (identified as Site I), subdomain IIIA (designated as Site II), and subdomain IB (recognized as Site III) within the HSA crystal structure (PDB: 1BM0). Each binding location underwent a total of 500 runs. Note that values ≤ 5 kJ mol^{-1} are not represented.

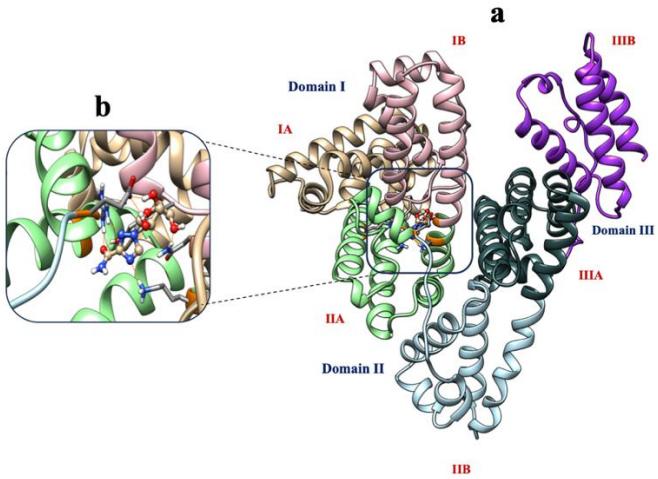

Fig. 3 – Orientation analysis of the RIB-HSA system (a) the binding orientation of RIB (shown in ball and stick) on Sudlow's Site I of HSA. The domains of HSA are colour-coded as follows: Domain I is represented in gold and pink, Domain II in light green and light blue, and Domain III in dark slate grey and purple. Zoomed-in image highlights the hydrogen bonds (depicted as orange lines) formed between HSA residues and RIB at Sudlow's Site I (b) of HSA.

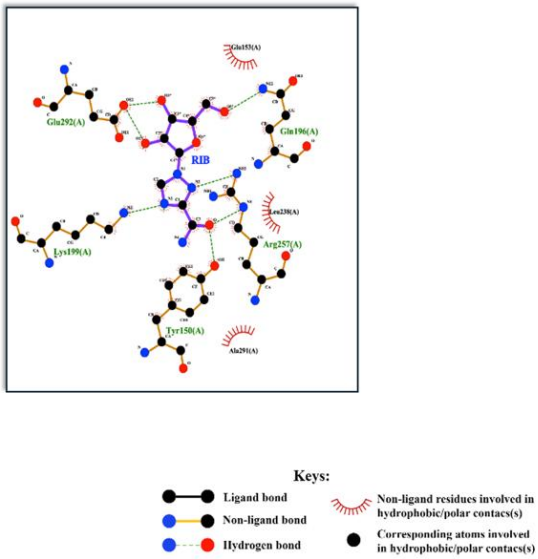

Fig. 4 – LigPlot+ diagram illustrating the hydrophobic interactions (in red) and polar interactions (in green) that occurred between RIB atoms and the amino acid residues of the protein at Site I.

Molecular dynamics (MD) simulation analysis

MD simulations were employed to explore the dynamic behaviour of the RIB-HSA interaction.[21] The system maintained an average temperature of 300 K and an average pressure of 0.96 bar when RIB was bound to Site I. In Fig. 5a, an initial observation suggests that the system remains stable, evidenced by an average total energy of approximately -1.5219 × 10^6 kJ mol^{-1}. This finding indicates that the ligand remained firmly attached to the protein throughout the simulation. Additionally, the distance between RIB and HSA during the simulation, as depicted in Fig. 5b, remained consistent, fluctuating around 0.2±0.05 nm throughout the entire MD simulations. These findings indicate that RIB consistently occupied the binding region on HSA's Site I.

As the simulation advanced, we further examined the stability of the HSA-RIB system based on the hydrogen bonds formed. However, the ratio of hydrogen bonds formed during the simulation fluctuated. There seems to be a total of nine H-bonds that might form between HSA and RIB in Site I. Consistently, in the simulation time frame, a minimum of four hydrogen bond interactions was observed, as indicated in Fig. 5c. Significantly, this suggests that these hydrogen bonds played a role in enhancing the binding affinity of RIB to HSA at Site I.

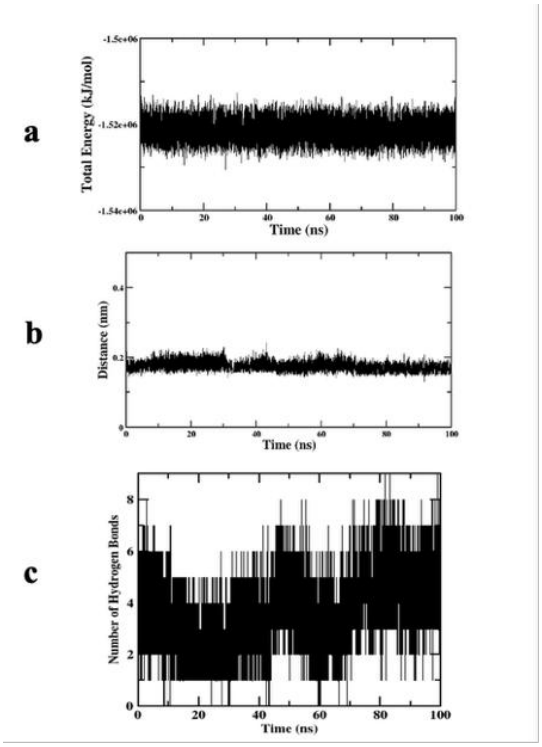

Fig. 5 – Graphs generated using XMGrace analysis for the RIB–HSA complex during 100 ns molecular dynamics simulations: a) Total energy profile indicating overall system stability; b) Distance between ribavirin and HSA showing consistent binding throughout the simulation. (c) Number of hydrogen bonds between RIB and HSA, demonstrating dynamic but sustained interaction across the trajectory.

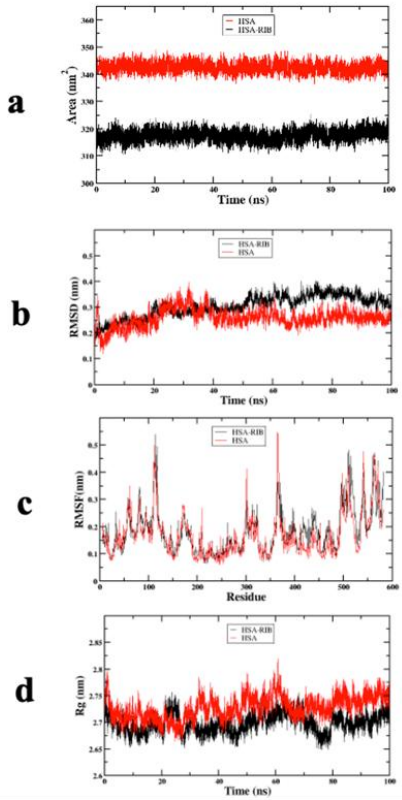

Fig. 6 – Graphs generated using XMGrace analysis comparing free HSA (red) and the RIB–HSA complex (black) during 100 ns molecular dynamics simulations: a) Solvent-accessible surface area (SASA) showing reduction upon RIB binding; b) Root mean square deviation (RMSD) indicating structural stability and equilibration; c) Root mean square fluctuation (RMSF) revealing residue-level flexibility; d) Radius of gyration (Rg) illustrating compactness of the protein structure over time.

In addition to hydrogen bonds, hydrophobic interactions are another non-covalent force that significantly contributes to the stability of a protein's native structure. These interactions are characterized by the solvent-accessible surface area (SASA), which describes the exposed surface area of a biomolecule to its surrounding solvent, including the van der Waals surface.[22] The plot in Fig. 6a shows the calculated SASA values for two simulation systems. Notably, the SASA values for HSA stabilized at 343 nm², while the binding of RIB to Site I of HSA reduced these values to approximately 315 nm².

In studies at the molecular scale, the root-mean-square deviation (RMSD) values of biomolecules, polymers, and long chains serve as a measure of the average distance between molecules and atoms within structures or clusters. Therefore, a consistent trend in RMSD values indicates that the simulated systems has reached equilibrium conditions.[23] The RMSD measurements for the Cα atoms of the unbound HSA and the RIB-HSA complex systems were evaluated throughout the 100 ns simulation period and depicted in Fig. 6b. Remarkably, it became apparent that all systems reached equilibrium after 20 ns. Notably, stabilization occurred for all systems beyond the initial 20 ns. The RMSD value for the RIB-HSA complex surpassed that of free HSA. The general trajectory of the RMSD for both RIB-HSA and HSA systems displayed an upward trend, with peak RMSD values of 0.4 nm and 0.35 nm, respectively. These values suggest that both systems underwent dynamic alterations in their structural framework. All systems overlapped during the simulation time of 5–43 ns. This may reflect increased atomic-level interactions of HSA atoms in the presence of RIB, leading to certain conformational and structural adjustments.

To monitor per-residue fluctuations, RMSF was calculated based on the Cα atoms. The RMSF, or root mean square fluctuation, measures how much each residue moves or fluctuates during the simulation.[24] In Fig. 6c, the computed RMSF of HSA and HSA-RIB complex for Site I were generated. During the 100 ns MD simulation, RIB remained firmly attached to HSA, indicating the stability of the resulting HSA structure upon RIB binding, assessing HSA's structural integrity using RMSF revealed regular flexibility (< 0.25 nm) for nearly all HSA residues.

The HSA-RIB complex shows high stability during simulation, except small fluctuations were noticed within residues 83–92, 197–205, 301–307, 400–426 and 523–537.

The radius of gyration (Rg), computed based on Cα atom positions, quantifies the compactness or expansion of a protein structure about its center of mass throughout time. It is derived from the root mean square distance of atoms within the structure from their collective center of mass.[25] The plot shows that all the system's Rg-time fluctuations were kept between 2.65 and 2.83 nm during the simulation. The RIB–HSA complex exhibited greater structural stability than HSA and retained compactness throughout the MD simulation time, with the exception of slight divergence observed between 67 and 70 ns (Fig. 6d). The results of all MD simulation analyses supported the docking findings and illustrated the stability of RIB when bound to Site I of HSA.

CONCLUSIONS

The findings obtained from this study indicated that RIB was bound to subdomain IIA (Site I) of HSA. The stabilizing forces for the formed complex were identified as hydrophobic and polar interactions, along with hydrogen bonds. At the same time, the MD simulation assessment suggested that the docked complex was relatively stable. These findings may offer valuable insights for further exploration in the context of HCV therapy studies.

Acknowledgement. We would like to express our gratitude to all those who helped us throughout this work.

REFERENCES

1. T. Bohnert, L. S. Gan, *J. Pharm. Sci.*, **2013**, *102*, 2953–2994. https://doi.org/10.1002/jps.23614
2. G. De Simone, A. di Masi, P. Ascenzi, *Int. J. Mol. Sci.*, **2021**, *22*, 10086. https://doi.org/10.3390/ijms221810086
3. D. Zhivkova, *Curr. Pharm. Des.*, **2015**, *21*, 1817–1830. https://doi.org/10.2174/1381612821666150302113710
4. N. J. Snell, *Expert Opin. Pharmacother*., **2005**, *2*, 1317–1324. https://doi.org/10.1517/14656566.2.8.1317
5. J. Huchting, Antivir. *Chem. Chemother.*, **2020**, *28*. https://doi.org/10.1177/2040206620976786
6. L. A. Bernal, V. Soti, *Cureus*, **2023**, *15*. https://doi.org/10.7759/cureus.43924
7. E. Thomas, M. G. Ghany, T. J. Liang, Antivir. Chem. Chemother., **2012**, 23, 1–12. https://doi.org/10.3851/IMP2125
8. M. Al-Nema, A. Gaurav, V. S. Lee, B. Gunasekaran, M. T. Lee, P. Okechukwu, *J. Mol. Liq.*, **2021**, *342*, 117485. https://doi.org/10.1016/j.molliq.2021.117485

9. N. E. Basken, C. J. Mathias, M. A. *Green, J. Pharm. Sci.*, **2009**, *98*, 2170–2179. https://doi.org/10.1002/jps.21570
10. Y. Li, Q. Meng, M. Yang, D. Liu, X. Hou, L. Tang, X. Wang, Y. Lyu, X. Chen, K. Liu, A. M. Yu, Z. Zuo, H. Bi, *Acta Pharm. Sin. B*, **2019**, *9*, 1113–1144. https://doi.org/10.1016/j.apsb.2019.10.001
11. Si. H. Fan, W. Q. Wang, Y. W. Zhou, X. J. Gao, Q. Zhang, M. H. Zhang, *Molecules*, **2024**, *29*, 655. https://doi.org/10.3390/molecules29030655
12. H.M. Berman, J. Westbrook, Z. Feng, G. Gilliland, T.N. Bhat, H. Weissig, I.N. Shindyalov, P.E. Bourne, *Nucleic Acid Research*, **2000**, 28: 235-242. https://doi.org/10.1093/nar/28.1.235
13. S. Sugio, A. Kashima, S. Mochizuki, M. Noda, K. Kobayashi, *Protein Eng.*, **1999**, 12, 439–446. https://doi.org/10.2210/pdb1BM0/pdb
14. S. E. Wong, F. C. Lightstone, *Expert Opin. Drug Discov.*, **2011**, *6*, 65–74. https://doi.org/10.1517/17460441.2011.534452
15. E. F. Pettersen, T. D. Goddard, C. C. Huang, G. S. Couch, D. M. Greenblatt, E. C. Meng, T. E. Ferrin, *J. Comput. Chem.*, **2004**, *25*, 1605–1612. https://doi.org/10.1002/jcc.20084
16. R. A. Laskowski, M. B. Swindells, *J. Chem. Inf. Model.*, **2011**, *51*, 2778–2786. https://doi.org/10.1021/ci200227u
17. S. Sasidharan, K. Radhakrishnan, J. Y. Lee, P. Saudagar, V. Gosu, D. Shin, *PLoS One*, **2023**, *18*. https://doi.org/10.1371/journal.pone.0283364
18. G. Bussi, D. Donadio, M. Parrinello, *J. Chem. Phys.*, **2007**, *126*, 014101. https://doi.org/10.1063/1.2408420
19. F. Sajadi, C. N. Rowley, *PeerJ*, **2018**, *6*, e5472. https://doi.org/10.7717/peerj.5472
20. M. Kožić, B. Bertoša, *NAR Genom. Bioinform.*, **2024**, *6*. https://doi.org/10.1093/nargab/lqad114
21. H. A. L. Filipe 1,2, L. M. S. Loura, *Molecules*, **2022**, *27*, 2105. https://doi.org/10.3390/molecules27072105
22. S. A. Ali, Md. I. Hassan, A. Islam, F. Ahmad, *Curr. Protein Pept. Sci.*, **2014**, *15*, 456–476. https://doi.org/10.2174/1389203715666140327114232
23. Z. K. Bagewadi, T. M. Yunus Khan, B. Gangadharappa, A. Kamalapurkar, S. M. Shamsudeen, D. A. Yaraguppi, *Saudi J. Biol. Sci.*, **2023**, *30*, 103753. https://doi.org/10.1016/j.sjbs.2023.103753
24. A. Amusengeri, Ö. Tastan Bishop, *Molecules*, **2019**, *24*, 188. https://doi.org/10.3390/molecules24010188
25. O. Soltanabadi, M. S. Atri, M. Bagheri, *J. Incl. Phenom. Macrocycl. Chem.*, **2018**, *91*, 189–197. https://doi.org/10.1007/s10847-018-0820-0